Angular Dependence for v', j'-Resolved States in $F + H_2 \rightarrow HF(v', j') + H$ Reactive Scattering Using a New Atomic Fluorine Beam Source

Gamini Dharmasena, Kyle Copeland, Joel H. Young, Rosemary A. Lasell, Timothy R. Phillips, Gregory A. Parker, and Mark Keil*

Department of Physics and Astronomy, University of Oklahoma, Norman, Oklahoma 73019-0225

Received: March 11, 1997; In Final Form: May 8, 1997[⊗]

Angular distributions are measured for individually resolved v', j' states of HF produced by $F + H_2 \rightarrow HF(v' = 1, j') + H$ and $F + H_2 \rightarrow HF(v'=2, j') + H$ reactive collisions in a crossed-beams scattering apparatus. Simultaneous resolution of the HF vibrational and rotational states is achieved spectroscopically for the first time, using laser excitation in conjunction with bolometric detection. The technique is sensitive to population differences between $v' = 1, j'$ and $v' = 2, j' - 1$ states optically coupled by specific $P_2(j')$ lines of a vib-rotational chemical laser. The measurements are greatly facilitated by the development of a new high-temperature atomic fluorine beam source, which exhibits excellent stability, very high intensity, and narrow velocity distributions. Features common to individual product rotational states are as follows: strong backward scattering into $v' = 2, j'$; weaker backward scattering into $v' = 1, j'$; and heretofore unobserved scattering into $v' = 1, j'$ in the forward hemisphere. These angular distributions agree qualitatively with predictions from fully three-dimensional exact quantum reactive scattering calculations (Castillo *et al*., *J. Chem. Phys*. **1996**, *104*, 6531) that were conducted on an accurate potential energy surface (Stark and Werner, *J. Chem. Phys*. **1996**, *104*, 6515). However, quasi-classical calculations conducted on the same potential energy surface do not produce any substantial forward-scattered HF in $v' = 1$ (Aoiz *et al*., *Chem. Phys. Lett*. **1994**, *223*, 215), suggesting that its appearance in the forward hemisphere may be a quantum effect. The quantum theoretical cross-sections also suggest that the forward $v' = 1$ products arise almost entirely from H_2 reactants initially in $j = 1$.

I. Introduction

Ever since the earliest molecular beam,[1] chemiluminescence,[2] and chemical laser[3] experiments, the $F + H_2$ reaction has been an important prototype for fundamental research in chemical reaction dynamics.[4] Its study has yielded tremendously insightful generalizations about reactive potential energy surfaces, detailed chemical kinetics, and energy disposal.[5,6] Increasingly detailed experimental and theoretical studies have enjoyed a symbiosis so successful that this reaction can now be investigated theoretically at the *ab initio* level using chemically accurate potential energy surfaces[7] and fully converged quantum dynamical calculations.[8]

Recent experimental studies bearing most directly on the $F + H_2$ reaction and its isotopic variants are exemplified by negative ion photodetachment spectra for the FH_2 reactive intermediate[9] and by vibrationally-resolved angular distribution measurements.[10,11] Corresponding theoretical investigations show clearly that the FH_2^- photodetachment spectra, and the detailed angular distributions, are exquisitely sensitive to the reactive potential energy surface.[12] Only for the $H(D) + H_2$ thermoneutral exchange reaction is a comparable level of experimental detail[13,14] and theoretical insight[15−19] accessible.

A recent review by Manolopoulos elegantly summarizes our current knowledge of $F + H_2$ reaction dynamics[12] and highlights the excellent match between the photodetachment experiments[9] and quantal predictions based on an accurate *ab initio* potential energy surface.[7] Furthermore, the quantal predictions[12,20] are largely in accord with vibrationally-resolved (but rotationally-unresolved) differential cross-section measurements.[10,11] It should be noted that although the photodetachment spectra directly probe the *shape* of the transition state region, they are not sensitive to the reaction barrier *height* with the experimental resolution that is currently available.[21]

Scattering experiments can provide very sensitive, albeit indirect, probes for the entrance and exit valleys of reactive potential energy surfaces and can therefore be complementary to the photodetachment studies. For reactive encounters, sampling of the transition state region is convoluted with entrance- and exit-channel effects. If the scattering event is nonreactive, the asymptotic regions may be probed separately.[22−24]

One of the major tenets of the scattering approach to reaction dynamics is the attempt to improve sensitivity to fundamental details of the potential energy surface by removing successive layers of convolution, just as cross-section measurements reduce translational energy averaging inherent in chemical kinetics and angular distribution measurements reduce averaging over classical impact parameters (or orbital angular momenta). For $F + H_2$ in particular, the need to correctly predict product vibrational distributions[2] led inexorably from high-quality semiempirical potential energy surfaces[25] to the most recent *ab initio* one.[7]

The measurement of *rotationally*-resolved angular distributions constitutes an important next step in reactive scattering studies and has been achieved for the $H + D_2$ reaction,[13,14] for $Cl + CH_4$, C_2H_6,[26] and other hydrocarbons,[27] but not for $F + H_2$ nor for any other exothermic chemical reaction. It is highly desirable to measure such v', j'-resolved products in order to reduce substantially the range of angular momenta (partial waves) that contribute to the observed cross-sections. This will improve prospects for observing reactive scattering resonances[21] and will provide more stringent tests for potential energy surfaces and dynamical calculations. In addition, calculated rotationally-resolved differential cross-sections for $F + H_2$ are strongly affected by the initial kinetic and rotational energy and

[⊗] Abstract published in *Advance ACS Abstracts,* July 15, 1997.

S1089-5639(97)00918-3 CCC: $14.00

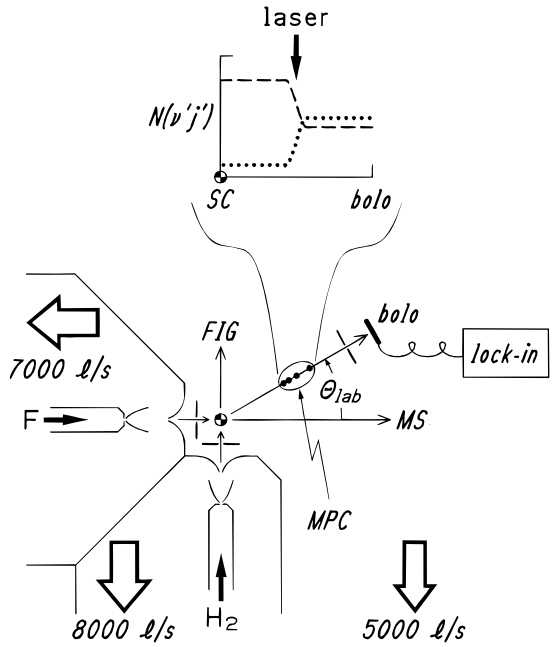

Figure 1. Schematic illustration of the scattering apparatus (top view). The two beam source chambers and the scattering chamber are pumped using independent vacuum systems denoted by the heavy arrows. The unscattered fluorine beam is monitored by a mass spectrometer (MS), while the H_2 beam is monitored by a fast ion gauge (FIG). Scattered HF products interact with the chemical laser in a multiple-pass cell (MPC). The inset shows the state-specific population of the products $[N(v', j')]$ as they travel from the scattering center (SC) to the bolometer detector (bolo). The laser decreases the population in $v' = 2$ by stimulated emission (dashed curve), thereby increasing the population in $v' = 1$ (dotted curve).

show substantial oscillatory structure.[28] There are also theoretical indications[8,18,29,30] that rotationally-resolved scattering will show prominent resonance or other quantum features.[12,28]

In section II of this paper, we provide detailed descriptions of the changes made to our crossed molecular beams apparatus,[31] enabling determination of angular distributions for reactive scattering that resolve product vibrational and rotational states simultaneously. Particularly helpful to the success of these measurements is the development of a new atomic fluorine source, which is described in section III. Averaging of theoretical differential cross-section calculations and simulations appropriate for laser + bolometer detection are described in section IV. Angular distribution measurements are presented and analyzed in section V, using fully-converged state-to-state quantum scattering calculations[8,28] conducted on an accurate *ab initio* potential energy surface.[7] Qualitative comparisons are also made to quasi-classical trajectory calculations conducted using the same potential energy surface.[32] Finally, we summarize our findings in section VI. We also anticipate future experiments measuring vibrationally and rotationally state-resolved angular distributions for reactively scattered HF using the methods developed in this study.

II. Scattering Apparatus

The experimental apparatus used for this study is shown schematically in Figure 1. Earlier versions of this apparatus have been used for rotationally inelastic scattering of HF[31] and for elastic differential cross-section measurements.[33,34] This description concentrates on changes that enable the apparatus to measure state-resolved angular distributions for reactive scattering.

A. Beam Sources. The apparatus consists of two supersonic molecular beam sources, each pumped independently by unbaffled diffusion pumps (Varian). Gas flows are regulated (Sierra), and the corresponding pressures are measured by capacitance manometers (MKS). Both beams are generated by continuous expansions through circular nozzles. No attempt is made to control the H_2 initial rotational distribution, which we assume is typical for strong supersonic expansions of *normal*-H_2.[35] The atomic fluorine beam is generated by thermal dissociation of molecular F_2 in a pyrolysis source specially developed for these experiments, the construction and characterization of which is detailed in section III. Operating characteristics and relevant apparatus dimensions for both beams are summarized in Table 1.

TABLE 1: Molecular Beam Operating Conditions

	F/He[a]	H_2
gas temp (K)	1199[b]	304
nozzle diam (mm)	0.15	0.03
nozzle pressure (atm)	4.9	29.8
flow (atm·cm^3/s)	8.3	11.7
nozzle−skimmer distance (mm)	21	10
skimmer diam (mm)	0.82	0.76
collimator diam (mm)	2.0	2.0
angular divergence (deg)[c]	2.2	4.3
nozzle-scattering center distance (mm)	41	30
most probable velocity (km/s)	3.01[b,d]	2.73[d]
velocity fwhm ($\Delta v/v_{mp}$)[d]	0.13	0.04[e]

[a] The atomic fluorine beam is generated from a mixture of 5% F_2 in He. [b] The gas temperature is obtained from the measured atomic F velocity, as discussed in section III.C. The experiments using the $P_2(6)$ laser excitation were run with a slightly faster beam, corresponding to a gas temperature of 1247 K and a most probable atomic F velocity of 3.07 km/s. [c] Calculated. [d] The most probable collision energy is 0.155 eV with an energy spread of 0.02 eV; the faster F beam used for the $P_2(6)$ experiments yields a collision energy of 0.158 eV. [e] This distribution was too narrow for our mass spectrometer to resolve and was instead estimated from similar beam expansion conditions for H_2 as reported in ref 10.

Both beams enter the scattering chamber directly from the source chambers, with no further differential pumping, and both have been moved much closer to the scattering center than in previous work. To reduce the amount of background gases that effuse from the source chambers to the scattering center, each beam passes through an additional (noncollimating) 2-mm-diameter aperture placed 3 mm beyond the skimmer base and just 5 mm before the scattering center. The collision zone therefore measures about 1.6 × 1.6 × 2.3 mm. During experiments, the pressure in the scattering chamber is maintained below $\sim 2 \times 10^{-6}$ Torr by an unbaffled diffusion pump.

Incident beam velocities, and the atomic F velocity distribution, are measured using a slotted disk and a mass spectrometer beam detector. The most probable collision energy is 0.155 eV, with a full-width at half-maximum (fwhm) spread of about 0.026 eV due mostly to the fast atomic F beam. Angular distributions for one experiment are reported using a slightly faster F beam, corresponding to a collision energy of 0.158 eV. It should be noted that the beam velocity distributions do not affect the product state resolution of the present experiment as they would for time-of-flight methods,[10,11] since the scattered HF is detected spectroscopically.

B. Bolometer Detector. Reactively scattered HF molecules are detected by a liquid-helium-cooled bolometer operating at 1.4 K. This detector is rotatable about the scattering center over an angular range from $\Theta_{lab} = -30$ to $+100°$ with respect to the atomic F source ($\Theta_{lab} = +90°$ places the detector directly opposite the H_2 source). Access to the relatively large range of negative angles is very useful for measuring HF scattered into the forward hemisphere in the center-of-mass (CM) frame

of reference (section IV) and is enabled by cutting back a large part of the differential pumping wall in the H_2 source chamber (Figure 1).

The basic detection principle is founded upon the optothermal laser + bolometer technique developed by Gough *et al*.[36] and continually refined by Miller and co-workers:[37] scattered molecules impinging upon the bolometer give up their kinetic and internal energy, which is seen as a dc signal. If a modulated laser beam excites some of the molecules on their way to the bolometer, selective amplification of this ac component gives a direct measure of the excited population.

The bolometer is mounted on a rotatable flange whose axis passes through the crossed-beams collision zone. Collimating apertures for the bolometer are 39 and 81 mm from the scattering center; each has a diameter of 2.4 mm. Molecules of HF that are headed through these collimators first encounter a narrow line width laser tuned to a specific $v' = 1, j' \leftrightarrow v' = 2, j' - 1$ molecular transition of HF. The laser is bright enough to saturate the transition[38] and results in equilibrating the $v' = 1$ and $v' = 2$ populations. The inset in Figure 1 depicts how the populations in these states are changed by interaction with the laser for a typical situation in which more reactively-scattered HF is produced in $v' = 2$ than in $v' = 1$. In such cases, the laser causes more transitions to occur by stimulated emission than by stimulated absorption, so the total energy content of the scattered HF is *reduced* by the laser. The bolometer output, which is proportional to the total heat influx, is then *lower* when the laser is on than when it is off. By chopping the laser and measuring the bolometer output and its phase on a lock-in amplifier, we obtain a measure of the population *difference* between the $v' = 1, j'$ and $v' = 2, j' - 1$ states of HF produced by the F + H_2 reactive collision at any particular scattering angle Θ_{lab} (section IV).

The spectroscopically-based experimental configuration described above offers some important advantages over scattering machines employing mass spectrometric detection, especially as applied to F + H_2 reactive scattering studies.[10,11] Quantum state resolution is obtained directly, instead of being obtained by applying conservation considerations to kinetic energy measurements. Direct spectroscopic detection permits automatic resolution of individual rotational states, which has not yet been achieved by time-of-flight methods,[11,39] except for the special case of Rydberg atom detection for H + D_2[14]. Also, the laser + bolometer technique for $v' = 2 \rightarrow v' = 1$ transitions is completely blind to background HF, which is all in $v = 0$, unlike mass spectrometers that are plagued by large background signals at $m/e = 20$ arising from fluorine that reacts with hydrogen adsorbed onto vacuum chamber walls.[10]

C. Laser and Multiple-Pass Cell. The laser used for these experiments is a continuous-wave HF chemical laser that has been described in previous work,[31,40] and only recent modifications to the optical layout will be described here. The laser and its excitation of scattered HF is shown in Figure 2. By keeping the cavity length sufficiently short, and the intracavity iris sufficiently small, the laser oscillates on just one single mode of a specific $v' = 1, j' \leftrightarrow v' = 2, j' - 1$ P-branch transition selected by the grating. By actively stabilizing the laser to an intracavity Lamb dip,[40] we obtain a line width of <5 MHz, as measured using a 150-MHz étalon (Burleigh). The laser power of 100−150 mW is monitored continuously using a mirror chopper. Finally, the laser is collimated to a diameter of about 2 mm and introduced into the scattering chamber through a well-baffled CaF_2 window. The laser propagates vertically through the scattering apparatus, *i.e*., perpendicular to the plane of the reactant molecular beams.

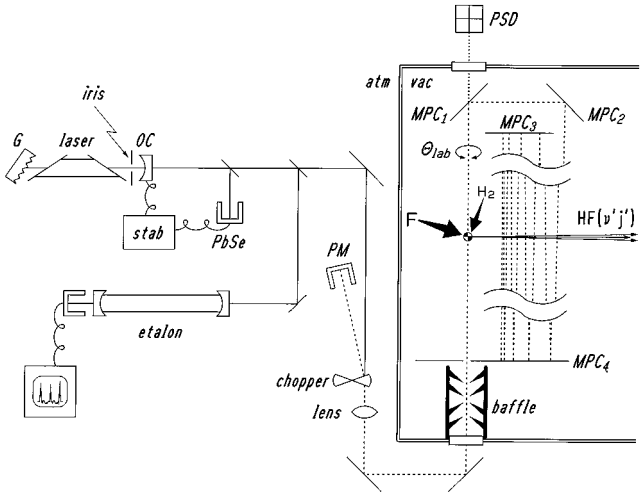

Figure 2. Schematic illustration of the chemical laser optical path and its interaction with reactively-scattered HF. The laser cavity consists of the diffraction grating (G), an intracvavity iris, and an output coupler (OC) whose position is controlled by active cavity stabilization (stab) using an infrared detector (PbSe). The laser output is monitored by an étalon and a power meter (PM). The mechanically chopped laser beam enters the scattering chamber along the rotation axis (Θ_{lab}) of the multiple-pass mirror assembly (MPC_1−MPC_4). The upper mirrors (MPC_1−MPC_3) may be rotated out of the laser path (dotted) for alignment using two position-sensitive detectors (PSD) located outside the vacuum chamber (only the lower PSD is shown).

Doppler broadening for the reactively-scattered HF, which is traveling at 3 km/s, is about 20 MHz per degree of angular divergence in the vertical direction. Consequently, the laser line width is sufficiently narrow that the only reactively-scattered HF that gets excited must be traveling within ±0.25° of horizontal. However, the bolometer aperture accommodates an angular range of ±1.4°. Consequently, we have designed a multiple-pass cell consisting of two plane mirrors (MPC_3 and MPC_4 in Figure 2), adjusted so that each pair of laser reflections tilts the laser 0.25° closer to vertical from the input laser beam. Two relay mirrors (MPC_1 and MPC_2) are used to adjust the input laser beam to 1.00° away from vertical. As the laser is reflected in a path progressively closer to the vertical direction, it interacts with scattered HF molecules whose velocities are correspondingly closer to horizontal. The final reflection in the multiple-pass cell is normal to the lower mirror, ensuring that the input laser radiation reemerges from the scattering apparatus (which helps reduce scattered light within the machine) and doubling the number of passes to 20. Using two position-sensitive pyroelectric detectors (Eltec), the infrared laser is aligned to within ±0.03 mrad and the bolometer detector rotation axis. This corresponds to a misalignment of the laser of ±0.15 mm as it returns from the multiple-pass cell, much smaller than any of our beams (all about 2 mm in diameter).

The laser and multiple-pass cell, in conjunction with the bolometer, comprise the entire optothermal[36] scattering detector. Rotating the multiple-pass cell and bolometer together then enables angular distributions for specified *vibrational and rotational* states of the reaction products to be measured *simultaneously*. A similar detection scheme, though without the multiple-pass cell, was successfully used to measure differential cross-sections for inelastic scattering of HF.[31] In the present case, however, using the bolometer is complicated by the presence of very intense beam sources so close to the scattering center, as we describe below.

D. Bolometer Responsivity. The bolometer detector has a stated responsivity of 1.5×10^6 V/W (Infrared Labs). During scattering experiments, the detector responsivity is reduced by

about a factor of 3 due to the thermal load of residual gas in the scattering chamber. This gas is distributed isotropically and therefore affects measurements equally at all scattering angles. However, for scattering angles $|\Theta_{lab}| \lesssim 9°$, the bolometer is also heated by the edge of the atomic beam (or by effusion from the source chamber), resulting in a strongly angle-dependent responsivity loss. Calibration experiments were conducted to determine how this reduced sensitivity affects measured signals due to laser-excited HF.

An isotropic background flux of HF was generated by inletting a small amount of the gas directly into the scattering chamber. With the H_2 beam turned off, an intense beam of pure He was then inlet through the F source to superimpose a strongly angle-dependent convective heat load on the bolometer. This arrangement simulated production of HF from the scattering experiment but with a distribution known to be isotropic. At each detector angle, the laser-induced bolometer signal and the bolometer responsivity were measured independently. The *ratio* of these two measurements was constant to within ±5%, as expected for an isotropic distribution of HF, even though both dropped to half their initial values near the He beam direction ($|\Theta_{lab}| = 6°$). Moreover, both the responsivity and the signal recovered fully as soon as the bolometer was rotated away from the He beam. These calibration measurements therefore demonstrate that measured bolometer signals may be linearized by using the detector responsivity.

For all angles $|\Theta_{lab}| \geq 7°$, the bolometer responsivity R and its signal S are measured sequentially. For the worst case at $\Theta_{lab} = \pm 7°$, the bolometer responsivity is reduced by about 20%, which is well within the calibrated range; no measurements are reported for scattering angles closer to the F beam than this.

The data reported here are calculated as the laser-induced *power* incident upon the bolometer, $P = S/R$, allowing more reliable measurements to be made over a wider angular range. We note that such power measurements are obtained directly in watts; since the HF vibrational transition energy is known, these measurements can be used to calculate the *absolute* molecular flux of HF. The calibrated laser + bolometer detection technique is complementary in this manner to the direct infrared absorption technique recently applied to rotationally inelastic scattering by Nesbitt and co-workers.[41]

E. Background Corrections. For the present experiments, modulated signals can be generated by scattered laser light, or (in principle) by HF impurities in the F beam. HF that is elastically scattered from H_2 must be in the ground vibrational state since the F source is operated well below the temperature required for significant vibrational excitation of HF. Also, the collision energy is insufficient to promote HF to $v = 1$ by inelastic scattering from H_2. Consequently, bolometer signals induced by $v' = 1 \leftrightarrow v' = 2$ transitions are completely free of interference from background HF, which can be a very troublesome source of noise for scattering experiments utilizing mass spectrometer detectors.[10,11] Background signals due to scattered laser light are removed by blocking the H_2 molecular beam before the scattering center and subtracting the signal from that obtained without blocking the H_2. It should be noted that the scattered light signals are 180° out-of-phase with respect to reactively-scattered HF whenever more HF is produced in $v' = 2$ than in $v' = 1$ (see inset to Figure 1).

III. Atomic Fluorine Source

In the present experiments, resolving individual rotational states for the HF product reduces the reactive flux into each state by at least an order of magnitude relative to rotationally-unresolved measurements for the F + H_2 reaction.[10,11] Calculated reactive differential cross-sections for the most populated $v' = 1, j'$ and $v' = 2, j'$ states are at most 0.03 and 0.08 Å^2/sr, respectively,[28] also an order of magnitude smaller than the weakest state-resolved differential cross-sections measured in previous work using laser + bolometer detection.[42,43] These considerations motivated our development of a new atomic fluorine source for the present scattering experiments, with the aim of improving its intensity drastically.

A. Methods for Generating Atomic Fluorine Beams. Two methods are commonly used for generating atomic F beams. A fluorine-containing gas is passed through either a microwave plasma discharge tube[44−48] or a heated metallic tube.[48,49] In the former case, the discharge pressure is too low to generate good supersonic expansions. Suitably narrow velocity distributions may be obtained using mechanical velocity selectors, but these typically lower the beam intensity by a further 1 or 2 orders of magnitude.[10] In chemical dynamics studies, it is more common to heat F_2, often diluted in an inert carrier gas,[11,50] to induce thermal dissociation into atomic F.

Maximum temperatures, and therefore maximum dissociation yields, are limited by the availability of materials capable of withstanding the corrosive action of fluorine at high temperatures; for example, only two metals are known to be suitable. For nickel, this maximum is 700−720 °C; at pressures required for good supersonic expansion, atomic dissociation yields are only 15% or less.[48] Fluorine rapidly destroys Ni at higher temperatures due to sublimation of the protective fluoride layer, and even lower dissociation yields (≈5%) are often tolerated to improve beam stability.[11] For iridium, temperatures exceeding 1500 °C can (in principle) be used, since its fluoride decomposes into the pure metal for temperatures exceeding 1500 °C.[51] Unfortunately however, this source has proven to be unstable and very difficult to use, because the Ir is rapidly destroyed at lower temperatures (where the fluoride is stable but gaseous), while any tube used to preheat the fluorine to 1500 °C would rapidly be destroyed in the 700−1500 °C temperature range.

Intense pulsed beams of atomic F have been generated by laser-induced dissociation of XeF_2[52] or SF_6.[53] However, both sources exhibit very broad translational energy distributions, and both suffer from very low duty cycles. Consequently, users of atomic F beams have been forced to compromise between (a) high dissociation yield, requiring a low-pressure gas and therefore sacrificing beam quality and intensity, or (b) high intensity, requiring high pressure and therefore sacrificing atomic dissociation yield. Both choices are unsatisfactory for producing a stable, intense source of atomic F.

Recently, we have shown that fluoride crystals of the Group II elements are chemically inert, and physically stable, in contact with hot fluorine for any temperature up to at least 1000 °C.[54] We have since developed and characterized an atomic F source based on a single-crystal tube of pure MgF_2,[55] which we describe here in detail. These sources have been adopted by several other research groups,[56,57] and MgF_2 nozzles have been incorporated into the most recent reactive scattering studies of Faubel and Toennies and their co-workers[11,58] subsequent to development in our laboratory.[55]

B. Source Design. Figure 3 shows the front end of the atomic F source used in the present experiments. The 14-cm-long MgF_2 tube is hollowed out from a single-crystal boule of optical-grade material (Optovac). The nozzle is drilled through the thin wall left at the end of the tube, forming an expansion channel about 1 mm long. The rear end of the tube is water-cooled and sealed with a Kalrez O-ring (DuPont) to a fluorine inlet at right angles to the tube axis. This allows visual

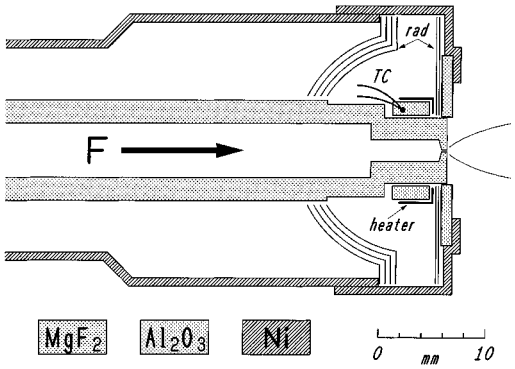

Figure 3. Scale view of the atomic fluorine source. The nozzle tip is heated indirectly by a Ta ribbon (heater) wrapped around an alumina collar whose temperature is measured and controlled (TC). Several layers of radiation shielding (rad) are used to ensure that the nozzle tip is the hottest part of the source. A sapphire disk at the front is used to protect the heater and radiation shields from excessive exposure to hot fluorine. Not shown are the heavy-gauge Ta electrical leads for the heater.

inspection of the nozzle through a sapphire window placed at the rear end of the source, even during operation.

Heating is provided by passing a 60-A current through a 0.1-mm-thick tantalum ribbon, dissipating about 150 W of ac power. The current is adjusted by a temperature controller (Fuji) using a thermocouple placed near the Ta heater and maintains the temperature stable to ±1 °C. The radiation shields and heater are protected from hot fluorine by sapphire and alumina, but they require periodic replacements in this extremely corrosive environment. The source chamber is pumped by two 16-in. diffusion pumps (Varian), backed by a Roots blower/rotary pump combination (Balzers). All pumps are charged with fully fluorinated oils and are purged continuously with dry nitrogen to inhibit corrosion. We have found it necessary to use two diffusion pumps since the Fomblin pumping fluid (with its very large molecular weight) halves the effective pumping speed.

Attaining the highest dissociation fraction possible requires the nozzle tip to be the hottest part of this source. Since the front end cannot be fully shielded against radiative heat loss (the expanding gas must be pumped away as rapidly as possible), it is necessary to allow substantial heat losses elsewhere and to impose a very steep thermal gradient right up to the nozzle. Indeed, radiation shielding that encloses the entire length of the tube reduces the required heater power, but the hottest point is then a region a few centimeters before the nozzle (see, for example, the highest-power curves in Figure 6 of ref 58). Observation through the sapphire viewport shows that this situation can result in sublimation of MgF_2 and gaseous transport to the cooler nozzle region, where the MgF_2 recrystallizes and progressively blocks the nozzle. The hemispherical radiation shielding presently in use (Figure 3) concentrates the radiant heater power right at the nozzle, while the surrounding Ni tube has slots cut along its length to enhance radiation losses further back. We no longer observe any crystalline growth within the tube, even at the highest temperatures, and test measurements conducted with pure He confirm that the nozzle is indeed the hottest point.

We also calibrated the nozzle temperature as monitored by the feedback thermocouple (Figure 3), the temperature of pure He flowing through the tube, and the actual gas temperature as found by measuring the He beam velocity. Although the external feedback thermocouple and the gas temperature inside the tube can differ by up to 100 °C, the temperature calculated from the He beam velocity is always within 10−20 °C of the internal temperature. Since we cannot measure the internal gas temperature when hot fluorine is flowing, the external thermocouple is used only to control the heater current; gas temperatures reported here are all calculated from beam velocity measurements.

TABLE 2: Atomic Fluorine Dissociation

controller[a] (K)	$P_{tot.}$[b] (Torr)	$F^+/F_2{}^+$ [c]	exp[d] (%)	v_F (km/s)	gas[e] (K)	α_{calc}[f] (%)
673	1941	0.31	0	2.033	567	0
873	2339	0.36	3	2.400	789	1
973	2546	0.57	17	2.589	912	5
1073	2766	1.28	42	2.792	1047	17
1173	2976	3.05	68	2.968	1169	38
1223	3041	5.31	79	3.056	1232	51
1273	3147	8.54	86	3.138	1295	64

[a] Temperature measured by the controller thermocouple (see Figure 3), located external to the MgF_2 tube. [b] Measured at the gas inlet. [c] Measurement errors are about ±3%. [d] Degree of dissociation calculated from eq 2 using the measured value of $\eta_0 = 0.31$ at 673 K. [e] Temperature calculated from the measured F velocity. At the lowest temperatures, the F_2 velocity is used instead; velocity measurements for $m/e = 19$ and 38 are indistinguishable. [f] Calculated using equilibrium constants given in ref 60 and the measured gas inlet pressure.

C. Atomic Dissociation Measurements. Other than beam intensity and velocity distributions, the most important source characteristic is the degree of thermal dissociation as a function of the gas temperature, commonly expressed as

$$\alpha = \frac{P_F}{P_F + 2P_{F_2}} \tag{1}$$

To measure this quantity, we need to account for dissociative ionization of F_2 to F^+ in the mass spectrometer ionizer. Following a procedure due to Miller and Patch,[59] we measure the F^+ and $F_2{}^+$ mass spectrometric intensities I as a function of the nozzle temperature. Their ratio, $\eta = I_{F^+}/I_{F_2{}^+}$, can be used to obtain the degree of thermal dissociation as

$$\alpha_{exp} \simeq \frac{\eta_T - \eta_0}{\eta_T + 1} \tag{2}$$

where we assume that transmission factors for F^+ and $F_2{}^+$ are approximately the same and that the cross-section for ionizing F is approximately half that for ionizing F_2.

Alternatively, the degree of dissociation can be calculated from the gas temperature, assuming equilibrium considerations. This temperature is determined from the peak of the F velocity distribution and is adjusted for the (temperature-dependent) average mass of the F/F_2/He gas mixture. Measured velocities for He are generally 2−3% faster than for fluorine due to slight velocity slippage, but no difference could be observed between measured velocities for F and F_2. The degree of dissociation may then be calculated using published values of the equilibrium constant[60] and the measured total pressure in the source at each temperature,

$$\alpha_{calc} = \frac{[K^2 + 16KP]^{1/2} - K}{8P} \tag{3}$$

where P is the initial partial pressure of F_2. Measurements pertaining to the calculation of beam gas temperatures and dissociation yields are collected in Table 2.

The calculated and experimental degrees of dissociation are compared in Figure 4, showing that an equilibrium sample of gas would be much less dissociated than observed. Rather than invoking temperature differences within the source,[58] which would require the temperature characteristic of dissociation to be about 150 °C *hotter* than the temperature characteristic of

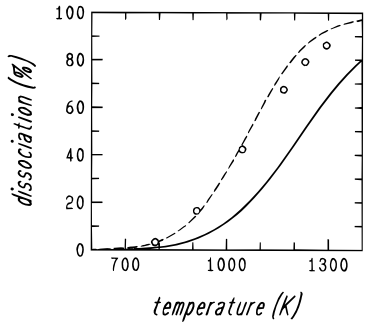

Figure 4. Measured yields (open circles) for dissociation of molecular into atomic fluorine, showing the dependence of α (eq 2) on the temperature obtained from the measured F velocity. The solid curve shows the dissociation yields calculated (eq 3) from known equilibrium constants[60] and the pressure measured at the source inlet. The dashed curve shows how the calculated dissociation yield would behave if the pressure were reduced by a factor of 10 during expansion through the nozzle (section III.C).

the beam gas velocity, it seems more likely that the effective (non-equilibrium) *pressure* controlling the dissociation is much lower than indicated by our measurements at the gas inlet. In particular, the gas pressure drops very rapidly as expansion occurs through the 1-mm-long nozzle channel (Figure 3), even though it certainly remains high enough to maintain thermal contact with the nozzle orifice. As can be seen from Figure 4, the measured dissociation curve can be modeled adequately if the pressure used in eq 3 is reduced by a factor of 10 from the measured inlet pressure.

The new source has proven to be robust, stable, and easy to use. Under conditions that would undoubtedly destroy Ni-based atomic F sources within minutes, our source remains completely immune to corrosion for the required duration of our longest-running experiments to date (10 h continuous). From a cold start, it can reach operating temperature in as little as 10 min (though we typically warm it up in 1 h), and the gas flow can be adjusted while the source is operating at any temperature: no passivation is required at all. It has been operated for gas temperatures up to 1050 °C, though more rapid sublimation of the nozzle tip into the vacuum causes earlier failure at higher temperatures. Best of all, the high temperatures now available for fluorine dissociation allow much higher nozzle pressures to be used, enabling much narrower velocity distributions and improving atomic F intensities by a factor of at least 10. We are also using these intense beams to etch semiconductor surfaces at rates comparable to those obtained using plasma discharge techniques, but with extremely straight walls characteristic of an atomic beam that experiences no gas-phase collisions.[61,62]

IV. Coordinate Transformations

In order to compare experimentally measured angular distributions to theoretically calculated differential cross-sections, it is necessary to transform one or the other to a common frame of reference. For most reactive-scattering experiments (but not all[63]), the laboratory frame measurements are transformed for comparison to theoretical calculations in the CM reference frame. These laboratory → CM transformations require best-fit deconvolution of instrumental averaging effects, such as beam velocity spreads and the detector angular resolution.[10] This deconvolution is best applied to scattering data with very high-resolution velocity measurements for the scattered products, since extracting a CM-frame differential cross-section for a single collision energy can otherwise result in misleading artifacts.[64]

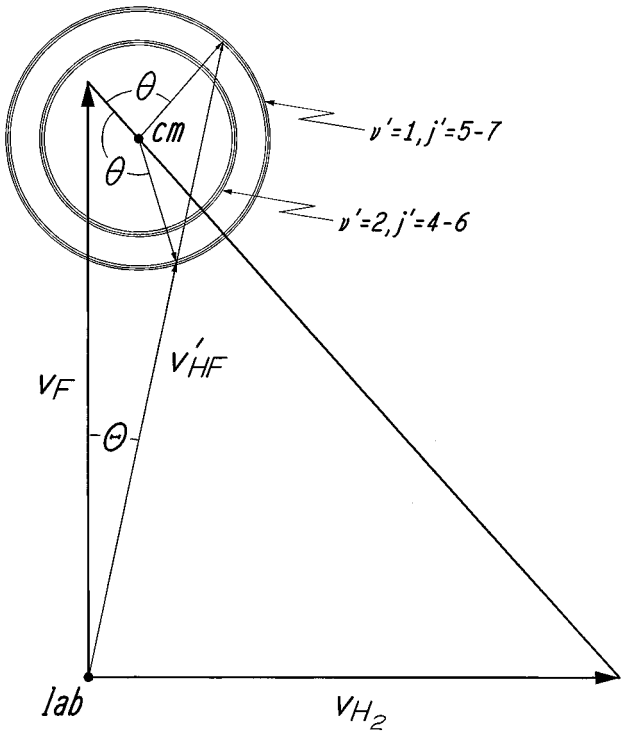

Figure 5. Velocity vector ("Newton") diagram showing a detector viewing molecules scattered through two different center-of-mass angles θ when positioned at a laboratory scattering angle Θ. The detector is assumed to be in the same plane as the reactant beams. Laboratory-frame velocity vectors are labeled "v"; a prime denotes the HF velocity after scattering. The Newton circles correspond to scattered HF in several rotational states of the $v' = 1$ (outer) and $v' = 2$ (inner) vibrational states. Laboratory-frame scattering angles are measured with respect to the F beam direction as shown. Center-of-mass scattering angles $\theta < 90°$ correspond to H-atom abstraction as the F flies by the H_2 and are conventionally referred to as "forward" scattering.

For conditions pertaining to the present experiment, the relation between scattering angles in the CM and laboratory reference frames is shown in the velocity vector ("Newton") diagram of Figure 5. Because the laboratory origin lies outside the Newton circles for reactively scattered HF, two CM scattering angles θ_{CM} contribute to measurements at any given laboratory-frame scattering angle Θ_{lab}. In the present experiments, these two contributions cannot be distinguished since we do not measure the velocity of the scattered products. (We note that resolving adjacent rotational states by time-of-flight methods would require a velocity solution better than 0.3%, or $\lesssim$7 meV.[11])

For the F + H_2 reaction, fully three-dimensional exact quantum state-to-state reactive differential cross-section calculations are now available[28] using an accurate potential energy surface:[7] in principle, there is no longer any need to perform laboratory → CM deconvolutions. Instead, we compare theory and experiment directly by transforming the calculated differential cross-sections into the laboratory frame and then perform a *forward* convolution over our instrumental parameters. This procedure completely avoids the above nonuniqueness problem[64] since the CM → laboratory transformation *is* unique.

Theoretical differential cross-sections for F + H_2 state-to-state reactive scattering[28] are transformed into the laboratory coordinate frame and averaged by means of Monte-Carlo integration[64] over the collision volume, the velocity distributions of the two beams, and the bolometer detector apertures. Further averaging effects over the rotational distribution of the incident H_2 are not included; as an approximation, all H_2 rotors are assumed to be in $j = 1$ initially. This choice is reasonable for

supersonically-cooled expansions of *normal*-H_2;[35] complete cooling would leave 75% in $j = 1$ and 25% in $j = 0$. Also, we do not average over the collision energy distribution, since the peak of the experimental distribution (0.155 eV) is somewhat higher than the highest collision energy (0.148 eV) available theoretically at the present time.[65]

The Monte-Carlo integration is performed for individual vibrational−rotational product states v', j' and yields simulated angular distributions $N_{v'j'}$ that are proportional to the number of product molecules impinging upon the detector per unit time. The power input to the bolometer is then

$$\text{power} = \frac{\text{molecules}}{\text{s}} \times \frac{\text{energy}}{\text{molecule}}, \quad \text{or} \quad P_{v'} = N_{v'j'}E_{v'j'} \quad (4)$$

where $E_{v'j'}$ is the total (translational and internal) energy of product molecules in state $v'j'$. Now consider the two states that are connected by a given laser transition, labeled 1 and 2. With the laser being chopped off and on successively, the corresponding power inputs to the bolometer, P_{off} and P_{on}, respectively, are

$$P_{\text{off}} = N_1E_1 + N_2E_2$$

$$P_{\text{on}} = N_1G_1E_1 + N_1G_2(E_1 + \Delta E) + N_2G_2E_2 + N_2G_1(E_2 - \Delta E) \quad (5)$$

where ΔE is the internal energy difference between these two states and $G_1 = g_1/(g_1 + g_2)$ and $G_2 = g_2/(g_1 + g_2)$ are corresponding rotational degeneracy factors giving relative populations in states 1 and 2 after interaction with a laser that fully saturates the $1 \leftrightarrow 2$ transition. The lock-in amplifier then extracts a modulated signal from the bolometer that is proportional to the power *difference* P_{diff} that is brought into the detector by molecules in the two states:

$$P_{\text{diff}} = P_{\text{off}} - P_{\text{on}} = (N_2G_1 - N_1G_2)\Delta E \quad (6)$$

We note that the modulated bolometer signal can be either positive ($N_2G_1 > N_1G_2$) or negative. This discussion also assumes that the laser transition is completely saturated and that polarization effects are unimportant. The former assumption has been shown to be valid for the laser power used in the present study,[38] while the latter assumption is reasonable for the present conditions of saturation and high rotational state degeneracies. No allowance is necessary for spontaneous emission, which is much slower than HF flight times to the detector. It should be noted that the laser-induced signal (eq 6) is entirely independent of the HF kinetic energy and of its heat of condensation upon freezing to the bolometer.

For each laser line, theoretically calculated angular distributions are appropriately weighted for $v' = 2 \rightarrow 1$ deexcitation (*i.e.*, $N_2G_1\Delta E$) and are separately weighted for $v' = 1 \rightarrow 2$ excitation (*i.e.*, $N_1G_2\Delta E$), as shown by the broken curves in Figure 6. The difference between these two curves then simulates the angular distributions measured by the laser + bolometer detector. The sign of this difference is arbitrary; for convenience we subtract the laser-on power from the laser-off power in eq 6 and render net deexcitation as a "positive" signal. The "negative" differences simulated in Figure 6 then correspond to scattering at angles where product HF in $v' = 1$ exceeds that in $v' = 2$. Generally, this occurs only for laboratory-frame scattering angles outside the $v' = 2$ Newton sphere, where HF is produced in $v' = 1$ exclusively.

V. Results and Discussion

A. Angular Distribution Measurements. Angular distributions are measured by averaging the laser-induced bolometer signal for scattering angles Θ_{lab} between −12 and +22° with respect to the incident atomic F beam, where $\Theta_{\text{lab}} = +90°$ refers to the direction of the incident H_2 beam. The Newton diagram in Figure 6 shows that this range of laboratory angles encompasses all scattering angles in the CM frame for the kinematics of the present experiment. At each scattering angle, generally spaced by 1 or 2° except near the atomic F beam (section II.D), the signal is averaged by a lock-in amplifier (Stanford Research) for 160 s. Half the measurement time is spent averaging the signal with the H_2 beam blocked; this background signal is due to scattered laser light and is subtracted from the signal measured with the unimpeded H_2 beam. For almost all scattering angles, the lock-in phase of the background signal is 180° out-of-phase with respect to the scattering signal; *i.e.*, the two contributions have opposite signs (for the purposes of this paper, 180° out-of-phase signals are arbitrarily defined as "positive").

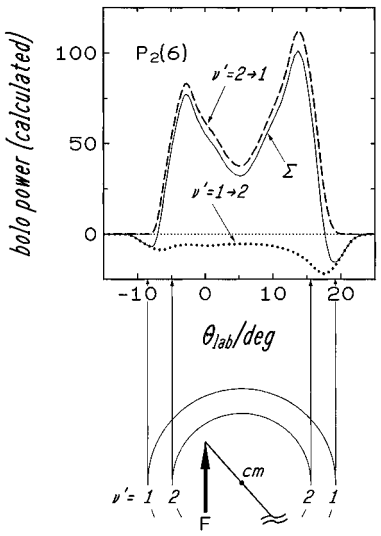

Figure 6. Simulated angular distributions calculated from fully-converged quantum theoretical calculations,[8] averaged over most experimental conditions (section IV) and separated into the contributions from $v' = 2 \rightarrow v' = 1$ deexcitation (dashed curve) and $v' = 1 \rightarrow v' = 2$ excitation (dotted curve). Both broken curves are appropriately weighted for the $j' = 5$ and $j' = 6$ rotational state degeneracies (eq 6). Also, the $v' = 1 \rightarrow v' = 2$ excitation curve has been inverted for convenience, so deexcitation is shown as a "positive" power incident upon the bolometer. The sum of these contributions (solid curve) can be compared directly to the bolometer power measurements. Also shown are the laboratory-frame angles within which scattering is confined kinematically, as depicted by tangents to the product state $v' = 1$ and $v' = 2$ Newton spheres.

Since scattered light must heat up the bolometer, the observed phase difference shows that we are measuring laser-induced *cooling*, *i.e.*, deexcitation of HF molecules. Since the laser is tuned for $v' = 1 \leftrightarrow v' = 2$ transitions, deexcitation can occur only if HF molecules incident upon the bolometer are in $v' = 2$ before interacting with the laser. This is an important signature of reactive scattering, since thermal excitation of $v' = 2$ is negligible.

In addition to the observed phase difference, several additional tests were conducted to verify the origin of the measured signals. Firstly, the signal disappears when we block the laser beam or either of the gas beams. This shows that the observed signals do not arise from HF present as background gas in the scattering chamber. Secondly, no scattering signal is seen when the fluorine source is cooled to 789 K, at which temperature there is almost no dissociation into atomic F (Table 2). This test also eliminates inelastically scattered HF (an impurity in the fluorine tank) as a possible contributor to the measured signal. Finally, no signals are observed outside the kinematically-

TABLE 3: Measured Angular Distribution[a]

	for given laser line		
Θ_{lab}	$P_2(5)$	$P_2(6)$	$P_2(7)$
−12.0	−1.5 ± 3.3	−0.5 ± 1.4	−2.2 ± 2.8
−10.0	−7.6 ± 0.6	−3.3 ± 2.6	0.3 ± 1.8
−9.0	−6.9 ± 2.6		
−8.0	−9.3 ± 2.8	−6.3 ± 0.8	−8.4 ± 2.6
−7.0	−3.1 ± 2.2		−7.1 ± 1.9
7.0	18.4 ± 2.4	22.8 ± 0.7	25.0 ± 1.0
8.0	29.2 ± 5.8	32.3 ± 1.8	27.9 ± 1.2
9.0	37.4 ± 1.6		36.8 ± 3.0
10.0	49.7 ± 3.0	48.6 ± 0.6	50.5 ± 2.2
11.0	56.7 ± 7.3	61.9 ± 0.5	57.2 ± 2.1
12.0	78.9 ± 5.9	71.5 ± 3.0	71.5 ± 0.9
13.0	91.1 ± 3.6	90.3 ± 1.1	85.8 ± 3.3
14.0[b]	100.0 ± 0.0	100.0 ± 0.0	100.0 ± 0.0
15.0	117.1 ± 5.8	88.2 ± 3.2	98.9 ± 7.3
16.0	107.0 ± 4.3	42.2 ± 4.5	61.6 ± 11.9
17.0	57.2 ± 5.7		12.9 ± 10.4
18.0	8.1 ± 0.5	−17.1 ± 1.3	−17.0 ± 1.1
19.0			−21.0 ± 0.5
20.0	−18.5 ± 3.2	−8.5 ± 0.7	−12.0 ± 1.5
22.0	−4.2 ± 0.6	0.6 ± 1.3	−2.2 ± 1.0

[a] Measured bolometer signals are adjusted by the measured bolometer responsitivity (section II.D). Signals reported as "positive" are 180° out-of-phase with respect to background scattered light signals and therefore corresponds to net deexcitation of HF molecules from $v' = 2$ to $v' = 1$; "negative" signals correspond to net excitation from $v' = 1$ to $v' = 2$. Error bars reflect 1 standard deviation. [b] Angular distributions for each laser line are arbitrarily normalized at $\Theta_{lab} = 14°$.

restricted range of laboratory-frame angles into which HF may be reactively scattered, $-12° \lesssim \Theta_{lab} \lesssim +22°$ (Figures 5 and 6).

In order to reduce signal fluctuations due to long-term drifts in beam intensities and detector sensitivity, we periodically (every $\approx 1/2$ h, or after 2−3 angles) measure the scattering signal at 14°, near the peak of the angular distributions. At each scattering angle we also measure the bolometer responsivity, which is used to calculate the laser-induced power arriving at the detector (section II.D). The strongest signals correspond to about 3×10^{-9} W, equivalent to the power carried by about 4×10^7 molecules/s impinging upon the bolometer, each deexcited by a single HF vibrational quantum.

Complete angular distributions for the laser tuned to $v' = 1 \leftrightarrow v' = 2$ transitions for three rotational states are collected in Table 3 and shown in Figure 7. The $P_2(5)$, $P_2(6)$, and $P_2(7)$ transitions are used because they are expected to probe the most populated rotational states in $v' = 2$.[10,11,28,66] Fortunately, they are also the strongest output lines for our chemical laser.[40]

The angular distributions shown are averages of two to four independent measurements at each scattering angle and laser line. Generally, the measurement errors are about ±2% of the reference intensity, except near the steep fall-off at $\Theta_{lab} = 15-18°$. Larger errors of ±5−10% for these angles are due to slow drifts in the atomic F velocity, which shifts the tangents to Newton spheres slightly for backward-scattered HF (Figures 5 and 6). The angular distributions for the three laser lines are normalized independently at $\Theta_{lab} = 14°$, so no comparison can be made relating their intensities.[67]

Each angular distribution shown requires 10−20 h of experimentation, including background subtraction and bolometer responsivity measurements. For the smaller scattering intensities (*e.g.*, $\Theta_{lab} \leq -7°$), the signal-to-noise ratio could be improved by longer integration times, since these intensities are still about 10 times larger than signals acquired in our earlier rotationally inelastic studies.[31]

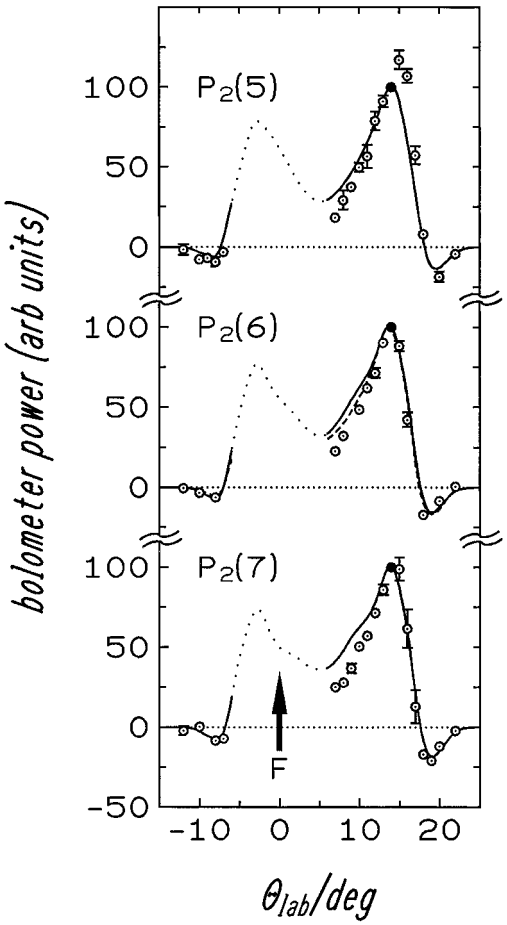

Figure 7. Experimental angular distributions (symbols) measured for $F + H_2$ reactive scattering using *P*-branch laser lines for three different vibrational−rotational transitions. Error bars (1 standard deviation) are shown only where they are larger than the symbols. Each distribution is independently normalized at the reference angle of $\Theta_{lab} = 14°$ (solid circle). The curves show fully-converged quantum theoretical calculations,[8] averaged over most experimental conditions (section IV) and scaled to the experiment at the reference angle. The dashed curve (shown only for the $P_2(6)$ results) simulates further averaging over an initial H_2 rotational distribution that is assumed to be rotationally cold *normal*-H_2 instead of purely in $j = 1$; this curve is barely discernable over most of the angular range. Scattering angles are measured with respect to the atomic fluorine beam (heavy arrow). The bolometer detector must stay at least 6° away from the incident fluorine beam (section II.D), so meaningful measurements cannot be made where the curves are dotted. The collision energy is 0.155 eV for the $P_2(5)$ and $P_2(7)$ experiments; the $P_2(6)$ experimental collision energy is 0.158 eV.

The angular distributions shown in Figure 7 are the first to resolve both the product vibrational and rotational states simultaneously for the $F + H_2 \rightarrow HF + H$ chemical reaction and are among only a handful of reactions for which this level of detail has been attained.[13,14,26,27,63] Besides the $H + D_2 \rightarrow HD + D$ reaction,[13,14] these measurements provide the only v', j' state-resolved angular distributions that can be compared to accurate quantum mechanical calculations[8] on an accurate potential energy surface.[7] Such a comparison is shown in Figure 7, where we display the calculated, fully-converged theoretical differential cross-sections after transforming to the laboratory frame, Monte-Carlo averaging, and simulating the laser-induced difference signals measured by the bolometer detector (section IV). These comparisons show very good qualitative agreement for all three product rotational states observed in our experiments.

For the $P_2(6)$ calculations, we also estimate the effect of neglecting initial $j \neq 1$ states in the H_2 beam. Except for

scattering angles of $\Theta_{lab} = 7-11°$, this simplification is evidently very reasonable, and our assumption of $j = 1$ as the only initial rotational state in our *normal*-H_2 beam does not significantly affect comparisons to the present experimental data.

B. Kinematic Features. The main features of all three observed angular distributions are most easily recognized by referring to a Newton diagram appropriate for the kinematics of this experiment (Figure 6). The sharp peak at $\Theta_{lab} = 14°$ occurs just inside the tangent to the $v' = 2$ Newton sphere and corresponds to scattering of HF(v'=2, j'=5) and HF(v'=1, j'=6) into the "backward" hemisphere (backward scattering refers to HF products scattered in a direction opposite the incident direction of F, in the CM frame). Since these signals are out-of-phase with respect to the laser chopper, they evidently correspond to net $v' = 2 \rightarrow v' = 1$ deexcitation. Conversely, the (negative) peak at $\Theta_{lab} = 19°$ is in-phase and therefore corresponds to net $v' = 1 \rightarrow v' = 2$ excitation. The sign reversal is expected since the faster $v' = 1$ products can be scattered more widely in the laboratory frame, and only these products can appear for scattering angles lying outside the range accessible to the slower $v' = 2$ products. The results for $\Theta_{lab} \geq 7°$ show that $v' = 1$ scattering is considerably weaker than $v' = 2$ scattering for the product rotational states considered here. Strong backward scattering for rotationally-unresolved HF products has previously been found in many studies of F + H_2 and its isotopic analogues,[10,11] for which $v' = 1$ is invariably weaker than $v' = 2$.

The third feature evident in Figure 7 is a (negative) peak at $\Theta_{lab} = -8°$, which lies close to the $v' = 1$ tangent in the forward scattering direction. Since this laboratory scattering angle lies beyond the tangent for $v' = 2$ scattering (which occurs at $\Theta_{lab} = -5°$), it corresponds to scattering of HF(v'=1) in the forward hemisphere, uncontaminated with any $v' = 2$ products. In a preliminary communication of the $P_2(6)$ data, we remarked that this is the first observation of foward scattering for $v' = 1$ products in F + H_2 reactive scattering.[68] Forward scattering has previously been observed for HF produced in $v' = 3$, which Neumark *et al.* originally took as evidence of dynamical resonances in reactive scattering.[10] However, once the Stark−Werner potential energy surface became available,[7] Aoiz and co-workers showed that most of the observed forward scattering into $v' = 3$ is reproduced by quasi-classical trajectory calculations.[32] Forward scattering for HF in $v' = 2$ was not observed in Neumark *et al.*'s high-resolution time-of-flight experiments despite an explicit search for it,[10] and $v' = 1$ products lie too far into negative laboratory-frame scattering angles for detection in those experiments. Conversely, the fast F beam used for the present experiments renders the $v' = 1$ products well within the angular range of our detector, but any $v' = 2$ products would lie too close to the incident F beam (dotted curves in Figure 7).

C. Comparison to Theory. In addition to the three main features discussed above, which are primarily kinematic in that they all appear near tangents to Newton spheres, comparing the measurements and the theoretical calculations suggests further significance in the present results. In order to interpret the measurements more reliably, it is very useful to relate scattering angles in the laboratory and CM reference frames, along with effects due to instrumental averaging. This relation is easily simulated by transforming and Monte-Carlo averaging an assumed differential cross-section that is nonzero only for a narrow cone of scattering angles in the CM frame. A number of such simulations over the entire range of $\Theta_{CM} = 0-180°$ is shown in Figure 8 for scattering into the $v' = 1$, $j' = 6$ product state and in Figure 9 for scattering into $v' = 2$, $j' = 5$. These simulations assume a 10°-wide angular cone in the CM frame,

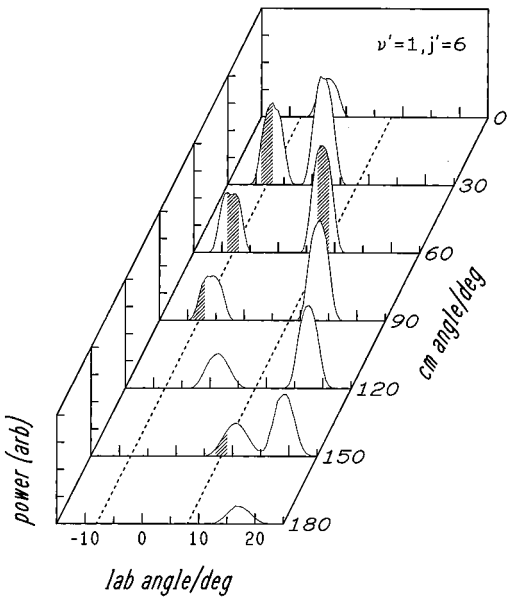

Figure 8. Perspective plot showing how a differential cross-section that is sharply peaked at $\theta_{CM} = 0°$, or 30°, or 60°, *etc.*, would appear when transformed to the laboratory frame and Monte-Carlo averaged over the collision volume, the velocity distributions of the two beams, and the bolometer detector apertures (section IV). The kinematics are appropriate for production of HF in the $v' = 1$, $j' = 6$ vibrational−rotational state. Dotted lines show how scattering at $\Theta_{lab} = \pm 8°$ relates to scattering in the CM (hatched regions). The width of the hatched regions gives the approximate (laboratory) angular resolution of the bolometer detector. The figure is especially convenient as a portrayal of the apparatus response function.

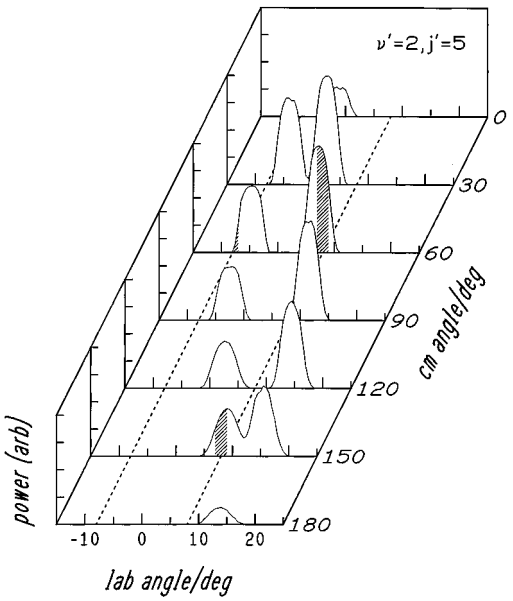

Figure 9. Same as Figure 8, but for HF produced in the $v' = 2$, $j' = 5$ vibrational−rotational state.

which roughly corresponds to the angular resolution of our detector in the laboratory frame (the ratio of laboratory to CM scattered velocities in Figure 5 is ≈5 for $v' = 1$ and ≈7 for $v' = 2$ at the laboratory scattering angle corresponding to the center of mass).

Of particular interest in these plots are laboratory angles near $\Theta_{lab} = -8°$, which correspond to the small negative peak in the observed angular distributions, and near $\Theta_{lab} = +8°$, which corresponds to discrepancies observed between the calculated and measured angular distributions shown in Figure 7. The hatched areas represent the entire range of laboratory angles seen by the detector placed at $\Theta_{lab} = \pm 8°$. Figure 8 shows

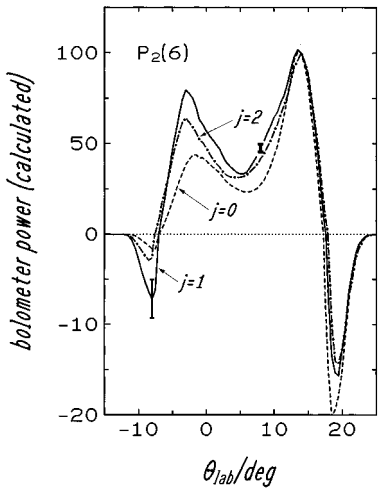

Figure 10. Angular distributions showing contributions to simulated bolometer signals for individual initial rotational states of H_2, based on theoretical state-to-state differential cross-sections.[28] Each angular distribution is independently normalized at $\Theta_{lab} = 14°$ for convenience in comparing to experimental data; without normalization the $j = 0$ angular distribution would be about 50% larger than the $j = 1$ or 2 distributions. The simulations are Monte-Carlo averaged over all apparatus distributions except for the collision energy spread and are summed over appropriately weighted $v' = 1$ and $v' = 2$ vibrational states (eq 6). "Negative" bolometer powers, corresponding to net $v' = 1 \rightarrow v' = 2$ laser-induced excitation, are increased by a factor of 5 for clarity of display. Error bars for measurements typical of the present experiments (Table 3) are shown at $\Theta_{lab} = \pm 8°$.

that the observed peak at $\Theta_{lab} = -8°$ is due to scattering into a range of CM angles from 30 to 90° (this range is unusually broad because $\Theta_{lab} = -8°$ is so near the $v' = 1$ tangent), while Figure 9 shows that very little of this scattering can be due to $v' = 2$. This substantiates our earlier qualitative conclusion based on Newton diagrams without instrumental averaging.[68]

The availability of theoretical differential cross-sections[8] allows us to examine the origin of $v' = 1$ forward scattering in somewhat more detail. In particular, calculations assuming rotationally state-selected H_2 beams are displayed in Figure 10 and predict that forward scattering is much weaker for $j = 0$ and $j = 2$ than for $j = 1$. This prediction and its verification may be especially significant, since quasi-classical trajectory calculations by Aoiz and co-workers simulating rotationally cold *normal*-H_2 show no $v' = 1$ products at CM scattering angles below about 60°, and only weak scattering in the 60−90° angular range.[32] The trajectories and the quantum scattering calculations employ the same Stark−Werner potential energy surface,[7] so the difference between their results cannot be attributed to discrepancies in potentials used for dynamical calculations.

We have also examined, as much as presently possible, how a more thorough simulation of our experimental conditions could affect the good agreement seen between the quantum predictions and the observed forward scattering. To partially evaluate the effect of our collision energy spread, we conducted additional simulations using quantum calculations available to us at the next lower collision energy of 0.112 eV.[28] The intensity of the $v' = 1$ forward scattering, and the initial state-specificity of its production by H_2 ($j = 1$), remain undiminished at the lower collision energy ($v' = 1$ forward scattering remains absent in the quasi-classical trajectory results at the lower collision energy). As already shown in Figure 7, simulating a reasonable distribution over H_2 initial rotational states also has no substantial effect upon the agreement between the quantum and experimental results. Consequently, it seems likely that the observed $v' = 1$ scattering in the forward hemisphere is a quantum mechanical effect and that it is due almost exclusively to reactant H_2 in the $j = 1$ rotational state. Given the experimental error presently attainable (Figure 10), the latter suggestion ought to be verifiable using a beam of *para*-H_2.[67]

Finally, we consider the lack of quantitative agreement between the quantum calculations and the measurements in the $\Theta_{lab} = 7-11°$ angular range. These disagreements are most evident for the $P_2(7)$ angular distribution, becoming smaller for the $P_2(6)$ experiment. For the $P_2(5)$ experiment, the agreement may actually be poorer than suggested by Figure 7, since the arbitrary factor required for normalizing the theoretical data to the experiment at $\Theta_{lab} = 14°$ appears to be too low. Figures 8 and 9 show that laboratory angles of $\Theta_{lab} = 8°$ correspond to CM angles in the vicinity of $\Theta_{CM} = 60°$ and/or $\Theta_{CM} = 150°$, for both product vibrational states. Although these two possible CM angles could be distinguished by measuring the laboratory-frame velocity of the scattered HF products, our experiments cannot accomplish such measurements. Also, it is possible that better simulation of the initial kinetic and rotational energy distributions will affect the apparent disagreement between theory and experiment (Figure 7). This will be resolved in dynamical calculations currently in progress,[65] while future experiments with improved resolution in the CM frame will allow more definitive examination of remaining disagreements between theory and experiment.

VI. Summary and Conclusions

We have developed and applied the laser + bolometer detection technique to reactive scattering, succeeding for the first time in measuring angular distributions for $F + H_2 \rightarrow HF + H$ that are resolved for both the product vibrational and rotational states simultaneously. These experiments also utilize a new high-temperature atomic fluorine beam source exhibiting excellent stability, very high intensity, and narrow velocity distributions. The source is characterized by much higher dissociation yields of F_2 than would be expected from equilibrium considerations. This departure appears to be due to the rapid drop in pressure during the (non-equilibrium) expansion through the hot nozzle.

The scattering results show good qualitative agreement with theoretical calculations that use both accurate quantum dynamics[8] and an accurate potential energy surface.[7] The high level of *ab initio* theoretical calculations for comparing to experimental investigations of fundamental chemical reaction dynamics has heretofore been achievable only for the $H + D_2$ exchange reaction.[14,69]

Despite limited angular resolution in the present experiments, the scattering results show several dynamical features previously unobserved in the $F + H_2$ reaction. Scattering of HF(v'=1) products into the forward hemisphere is measured for the first time. This scattering is reproduced by the quantum calculations very well, but not by quasi-classical trajectory calculations[32] conducted on the same potential energy surface. Consequently, it seems likely that the observed $v' = 1$ scattering into the forward hemisphere is a quantum mechanical effect. Furthermore, the quantum theoretical calculations suggest that this scattering is due almost exclusively to reactant H_2 in the $j = 1$ rotational state.

Our experiments to date have utilized fluorine beams seeded in He. This choice is made in order to maximize beam intensity and thereby improve the experimental sensitivity. In this context, it is worthwhile to note that some measurements reported here (*e.g.*, at $\Theta_{lab} = -8°$) correspond to state-to-state differential cross-sections theoretically calculated to be as small as 5×10^{-3} Å^2/sr.[28] Coincidentally however, the fast He-seeded

beam confines product HF to a rather narrow range of scattering angles in the laboratory frame, which improves the signal strength in that range at the cost of poorer angular resolution in the CM frame. Subsequent experiments will slow down the F by seeding in He/Ar mixtures, lowering the collision energy to values comparable to those used in earlier studies,[10] and simultaneously improving the CM-frame angular resolution. By studying the reactivity of *para*-H_2, the techniques developed in the present work can now be extended to the long-sought goal of measuring angular distributions for the completely specified vib-rotational state to vib-rotational state reactive scattering process for F + H_2(v=0, j) → HF(v', j') + H. These detailed experimental studies will be supported and guided by fully-converged exact quantum dynamical calculations[29,70] that we will conduct[65] on the most accurate potential energy surface available for the important F + H_2 prototype chemical reaction.

Acknowledgments. We are grateful to David Manolopoulos and to Jesus Castillo (Oxford) for providing their calculations of state-resolved differential cross-sections for F + H_2 reactive scattering and to Russ Pack and Bob Walker (Los Alamos) for providing their Monte-Carlo transformation-averaging code. We also appreciate many enjoyable and insightful discussions with Neil Shafer-Ray (Oklahoma) regarding state-to-state angular distributions in reactive scattering studies. It is a pleasure to thank Kirill Shokhirev for assistance with the simulation programs and Tina Patrick for help in designing the multiple-pass cell. We also thank Bob Littell and Barry Bergeron for their expert machining assistance and Dick Scott for his electronics design expertise. This research was supported by grants from the National Science Foundation under Grant No. CHE-9405005 and by the University of Oklahoma Research Council. Acknowledgement is also made to the donors of the Petroleum Research Fund, administered by the American Chemical Society, for partial support of this research. Finally, we wish to thank the organizers of the international symposium held in Taipei on "Modern Trends in Chemical Dynamics" in December 1996: it was a great privilege to see the abundant respect and affection of students and associates for Prof. Y. T. Lee.

References and Notes

(1) Schafer, T. P.; Siska, P. E.; Parson, J. M.; Tully, F. P.; Wong, Y. C.; Lee, Y. T. *J. Chem. Phys.* **1970**, *53*, 3385.

(2) Polanyi, J. C.; Woodall, K. B. *J. Chem. Phys.* **1972**, *57*, 1574.

(3) Coombe, R. D.; Pimentel, G. C. *J. Chem. Phys.* **1973**, *59*, 251.

(4) Levine, R. D.; Bernstein, R. B. *Molecular Reaction Dynamics and Chemical Reactivity*; Oxford University Press: Oxford, U.K., 1987.

(5) Polanyi, J. C. *Chem. Scr.* **1987**, *27*, 229.

(6) Herschbach, D. R. *Chem. Scr.* **1987**, *27*, 327.

(7) Stark, K.; Werner, H.-J. *J. Chem. Phys.* **1996**, *104*, 6515.

(8) Castillo, J. F.; Manolopoulous, D. E.; Stark, K.; Werner, H.-J. *J. Chem. Phys.* **1996**, *104*, 6531.

(9) Bradforth, S. E.; Arnold, D. W.; Neumark, D. M.; Manolopoulos, D. E. *J. Chem. Phys.* **1993**, *99*, 6345.

(10) (a) Neumark, D. M.; Wodtke, A. M.; Robinson, G. N.; Hayden, C. C.; Lee, Y. T. *J. Chem. Phys.* **1985**, *82*, 3045. (b) Neumark, D. M.; Wodtke, A. M.; Robinson, G. N.; Hayden, C. C.; Shobatake, K.; Sparks, R. K.; Schafer, T. P.; Lee, Y. T. *J. Chem. Phys.* **1985**, *82*, 3067.

(11) (a) Faubel, M.; Rusin, L.; Schlemmer, S.; Sondermann, F.; Tappe, U.; Toennies, J. P. *J. Chem. Phys.* **1994**, *101*, 2106. (b) Faubel, M.; Martinez-Haya, B.; Rusin, L.; Tappe, U.; Toennies, J. P. *Chem. Phys. Lett.* **1995**, *232*, 197.

(12) Manolopoulos, D. E. *J. Chem. Soc., Faraday Trans.* **1997**, *93*, 673.

(13) Xu, H.; Shafer-Ray, N. E.; Merkt, F.; Hughes, D. J.; Springer, M.; Tuckett, R. P.; Zare, R. N. *J. Chem. Phys.* **1995**, *103*, 5157.

(14) (a) Schnieder, L.; Seekamp-Rahn, K.; Borkowski, J.; Wrede, E.; Welge, K. H.; Aoiz, F. J.; Bañares, L.; D'Mello, M. J.; Herrero, V. J.; Sáez Rábanos, V.; Wyatt, R. E. *Science* **1995**, *269*, 207. (b) Wrede, E.; Schnieder, L. *J. Chem. Phys.*, in press.

(15) Zhang, J. Z. H.; Miller, W. H. *J. Chem. Phys.* **1989**, *91*, 1528.

(16) Neuhauser, D.; Judson, R. S.; Kouri, D. J.; Adelman, D. E.; Shafer, N. E.; Kliner, D. A. V.; Zare, R. N. *Science* **1992**, *257*, 519.

(17) Mielke, S. L.; Friedman, R. S.; Truhlar, G. D.; Schwenke, D. W.; Kouri, D. J. *Chem. Phys. Lett.* **1992**, *359*, 359.

(18) (a) Kuppermann, A.; Wu, Y.-S. M. *Chem. Phys. Lett.* **1995**, *241*, 229. (b) Kuppermann, A.; Wu, Y.-S. M. *Chem. Phys. Lett.* **1993**, *205*, 577.

(19) *Phys. Today* **1993**, (Mar), 17.

(20) Baer, M.; Faubel, M.; Martinez-Haya, B.; Rusin, L. Y.; Tappe, U.; Toennies, J. P. *J. Chem. Phys.* **1996**, *104*, 2743.

(21) Russell, C. L.; Manolopoulos, D. E. *Chem. Phys. Lett.* **1996**, *256*, 465.

(22) Faubel, M.; Rusin, L. Y.; Schlemmer, S.; Sondermann, F.; Tappe, U.; Toennies, J. P. *J. Chem. Soc., Faraday Trans.* **1993**, *89*, 1475.

(23) Lindner, J. L.; Lundberg, J. K.; Lovejoy, C. M.; Leone, S. R. *J. Chem. Phys.* **1997**, *106*, 2265.

(24) Schatz, G. C. *J. Chem. Phys.* **1997**, *106*, 2277.

(25) (a) Lynch, G. C.; Halvick, P.; Zhao, M.; Truhlar, D. G.; Yu, C.-H.; Kouri, D. J.; Schwenke, D. W. *J. Chem. Phys.* **1991**, *94*, 7150. (b) Mielke, S. L.; Lynch, G. C.; Truhlar, D. G.; Schwenke, D. W. *Chem. Phys. Lett.* **1993**, *213*, 10.

(26) (a) Simpson, W. R.; Rakitzis, T. P.; Kandel, S. A.; Orr-Ewing, A. J.; Zare, R. N. *J. Chem. Phys.* **1995**, *103*, 7313. (b) Kandel, S. A.; Rakitzis, T. P.; Lev-On, T.; Zare, R. N. *J. Chem. Phys.* **1996**, *105*, 7550. (c) Orr-Ewing, A. J.; Simpson, W. R.; Rakitzis, T. P.; Kandel, S. A.; Zare, R. N. *J. Chem. Phys.* **1997**, *106*, 5961.

(27) (a) Varley, D. F.; Dagdigian, P. J. *J. Phys. Chem.* **1995**, *99*, 9843. (b) Varley, D. F.; Dagdigian, P. J. *J. Phys. Chem.* **1996**, *100*, 4365.

(28) Manolopoulos, D. E. Private communication, 1996. We thank Prof. Manolopoulos and Jesus Castillo for kindly providing F + H_2 → HF(v', j') + H differential cross-sections calculated using the Stark−Werner potential energy surface.[7]

(29) (a) Bačić, Z.; Kress, J. D.; Parker, G. A.; Pack, R. T. *J. Chem. Phys.* **1990**, *92*, 2344. (b) Kress, J. D.; Bačić, Z.; Parker, G. A.; Pack, R. T. *Chem. Phys. Lett.* **1989**, *157*, 484. (c) Kress, J. D.; Pack, R. T.; Parker, G. A. *Chem. Phys. Lett.* **1990**, *170*, 306.

(30) D'Mello, M.; Manolopoulos, D. E.; Wyatt, R. E. *Chem. Phys. Lett.* **1990**, *168*, 113.

(31) Rawluk, L. J.; Fan, Y. B.; Apelblat, Y.; Keil, M. *J. Chem. Phys.* **1991**, *94*, 4205.

(32) Aoiz, F. J.; Bañares, L.; Herrero, V. J.; Sáez Rábanos, V.; Stark, K.; Werner, H.-J. *Chem. Phys. Lett.* **1994**, *223*, 215.

(33) Danielson, L. J.; McLeod, K. M.; Keil, M. *J. Chem. Phys.* **1987**, *87*, 239.

(34) Danielson, L. J.; Keil, M. *J. Chem. Phys.* **1988**, *88*, 851.

(35) Pollard, J. E.; Trevor, D. J.; Lee, Y. T.; Shirley, D. A. *J. Chem. Phys.* **1982**, *77*, 4818.

(36) Gough, T. E.; Miller, R. E.; Scoles, G. *Appl. Phys. Lett.* **1977**, *30*, 338.

(37) Bemish, R. J.; Wu, M.; Miller, R. E. *Faraday Discuss. Chem. Soc.* **1994**, *97*, 57.

(38) Fan, Y. B.; Rawluk, L. J.; Apelblat, Y.; Keil, M. *J. Opt. Soc. Am. B* **1991**, *8*, 1218.

(39) Continetti, R. E.; Balko, B. A.; Lee, Y. T. *J. Chem. Phys.* **1990**, *93*, 5719.

(40) Rawluk, L. J.; Keil, M. *J. Opt. Soc. Am. B* **1989**, *6*, 1278.

(41) (a) Chapman, W. B.; Schiffman, A.; Hutson, J. M.; Nesbitt, D. J. *J. Chem. Phys.* **1996**, *105*, 3497. (b) Chapman, W. B.; Weida, M. J.; Nesbitt, D. J. *J. Chem. Phys.* **1997**, *106*, 2248.

(42) Rawluk, L. J.; Keil, M.; Alexander, M. H.; Mayne, H. R.; Barrett, J. J. C. *Chem. Phys. Lett.* **1993**, *202*, 291.

(43) Keil, M.; Rawluk, L. J.; Alexander, M. H.; Mayne, H. R.; Barrett, J. J. C. *SPIE Proc.* **1994**, *2124*, 28.

(44) Gorry, P. A.; Grice, R. *J. Phys. E* **1979**, *12*, 857.

(45) Aquilanti, V.; Luzzatti, E.; Pirani, F.; Volpi, G. G. *Chem. Phys. Lett.* **1982**, *90*, 382.

(46) Schwalm, U. *Appl. Phys. B* **1983**, *30*, 149.

(47) Stinespring, C. D.; Freedman, A.; Kolb, C. E. *J. Vac. Sci. Technol. A* **1986**, *4*, 1946.

(48) Winters, H. F.; Coburn, J. W. *Surf. Sci. Rep.* **1992**, *14*, 164.

(49) Valentini, J. J.; Coggiola, M. J.; Lee, Y. T. *Rev. Sci. Instrum.* **1977**, *48*, 58. These authors describe a source for chlorine and bromine atomic beams using heated graphite tubes, which are replaced by pure nickel for use with fluorine.

(50) Sparks, R. K.; Hayden, C. C.; Shobatake, K.; Neumark, D. M.; Lee, Y. T. In *Horizons in Quantum Chemistry*; Fukui, K., Pullman, B., Eds.; Reidel: Dordrecht, The Netherlands, 1980; p 91.

(51) (a) Geis, M. W.; Efremow, N. N.; Lincoln, G. A. *J. Vac. Sci. Technol. B* **1986**, *4*, 315. (b) Geis, M. W.; Efremow, N. N.; Pang, S. W.; Anderson, A. C. *J. Vac. Sci. Technol. B* **1987**, *5*, 363.

(52) Levis, R. J.; Waltman, C. J.; Cousins, L. M.; Copeland, R. G.; Leone, S. R. *J. Vac. Sci. Technol. A* **1990**, *8*, 3118.

(53) Giapis, K. P.; Moore, T. A.; Minton, T. K. *J. Vac. Sci. Technol. A* **1995**, *13*, 959.

(54) Ericson, T.; Copeland, K.; Keil, M.; Apelblat, Y.; Fan, Y. B. *Rev. Sci. Instrum.* **1994**, *65*, 3587.

(55) Keil, M.; Young, J. H.; Copeland, K. U.S. Patent 5,597,495 (filed Nov 7, 1994). Copy available on request to M.K.

(56) Blank, D. A. Private communication, Berkeley, 1996.

(57) Chapman, W. B. Private communication, Colorado, 1997.

(58) Faubel, M.; Martinez-Haya, B.; Rusin, L. Y.; Tappe, U.; Toennies, J. P. *J. Phys. D* **1996**, *29*, 1885.

(59) Miller, D. R.; Patch, D. F. *Rev. Sci. Instrum.* **1969**, *40*, 1566.

(60) Trotman-Dickenson, A. F. *J. Chem. Soc.* **1959**, 3088.

(61) Copeland, K. A. M.Sc. Thesis, University of Oklahoma, 1995.

(62) Copeland, K.; Larson, P. R.; Lasell, R. A.; Dharmasena, G.; Johnson, M. B.; Keil, M. To be submitted for publication in *J. Vac. Sci. Tech. A.*

(63) Lai, L.-H.; Wang, J.-H.; Che, D.-C.; Liu, K. *J. Chem. Phys.* **1996**, *105*, 3332.

(64) Pack, R. T. *J. Chem. Phys.* **1984**, *81*, 1841.

(65) Phillips, T. R.; Dharmasena, G.; Keil, M.; Parker, G. A. Work in progress.

(66) (a) Launay, J. M. *Theor. Chim. Acta* **1991**, *79*, 183. (b) Launay J. M.; LeDourneuf, M. *Chem. Phys. Lett.* **1990**, *169*, 473.

(67) Dharmasena, G.; Phillips, T. R.; Keil, M.; Parker, G. A. Work in progress.

(68) Dharmasena, G.; Phillips, T. R.; Shokhirev, K. N.; Parker, G. A.; Keil, M. *J. Chem. Phys.*, in press.

(69) Shafer-Ray, N. E.; Xu, H.; Zare, R. N.; Kuppermann, A. Work in progress.

(70) (a) Parker, G. A.; Laganà, A.; Croccianti, S.; Pack, R. T. *J. Chem. Phys.* **1995**, *102*, 1238. (b) Pack, R. T.; Butcher, E. A.; Parker, G. A. *J. Chem. Phys.* **1995**, *102*, 5998.